Design and implementation of a 38 kW dish-Stirling concentrated solar power system

J Yan[1], Y D Peng[1,3], Z R Cheng[1], F M Liu[1] and X H Tang[2]

[1]Hunan Provincial Key Laboratory of Health Maintenance for Mechanical Equipment, Hunan University of Science and Technology, Xiangtan 411201, Hunan Province, China
[2]Solar Business Department of Xiangtan Electric Manufacturing Group, Xiangtan 411101, Hunan Province, China

E-mail: ydpeng@hnust.edu.cn

Abstract. Dish-Stirling concentrated solar power system (DS-CSP) is an important pathway for converting solar energy into electricity at high efficiency. In this study, a rated power 38 kW DS-CSP system was developed (installed in Xiangtan Electric Manufacturing Group). The heat engine adopted the alpha-type four cylinders double-acting Stirling engine (Stirling Biopower Flexgen S260). The absorber flux distribution simulation was conducted using ray tracing method and then the 204 m^2 parabolic dish concentrator system (diameter is 17.70 m and focal length is 9.49 m) with single concentrator plus single pillar supporting has been designed and built. A water-cooled disc target and an absorber imitation device were adopted to test the tracking performance of the dish concentrator system, homogeneity of the focal spot and flux distribution of the absorber. Finally, the S260 Stirling engine was installed on the focal position of the dish concentrator and then the net output power date of the 38 kW DS-CSP system was tested. The absorber overheating problem on the DS-CSP system performance was discussed when the DS-CSP system was installed in different locations. The testing result shows that this system achieved the net output power of 38 kW and solar-to-electricity efficiency (SEE) of 25.3% with the direct normal irradiation (DNI) at 750 W/m^2. The net output power can further increase to 40.5 kW with the SEE of 26.6% when the DNI reaches up to the maximum of 761 W/m^2. The net output power of the 38 kW DS-CSP system has a linear function relationship with the DNI. The fitting function is Net power output=0.1003×DNI－36.129, where DNI is at the range of 460~761 W/m^2. This function could be used to predict the amount of the 38 kW DS-CSP system annual generation power.

1. Introduction

Solar thermal power generation utilizes the sun as a heat source which can drive a heat engine for power production by concentrating technologies [1]. At present, Concentrated Solar Power technologies majorly include the solar tower system, Dish-Stirling concentrated solar power system (DS-CSP), parabolic trough system and Fresnel system [2]. The DS-CSP system is characterized by high solar-electricity efficiency, scalable power generation and high modularity, which has been regarded as a promising CSP technology for highly efficient solar power generation [3,4].

DS-CSP system consists of a parabolic concentrator and a Stirling engine system [5,6]. The parabolic concentrator provides highly concentrated solar irradiation as the heat source for the Stirling engine to produce electricity with a high efficiency which in turn achieves a high solar-to-electricity

efficiency [2,3,7-14]. The DS-CSP unit with world maximum output power was built by Schlaich-Bergermann und Partner Company (SBP). The diameter of the single dish parabolic concentrator is 17.0 m with a metal tensioned membrane structure. The maximum output power can reach 53 kW (direct normal irradiation (DNI) is 1000 W/m^2) with the 4-275 kinematic Stirling engine (rated power 50 kW) and the solar-to-electricity efficiency (SEE) is 23.0% [8,9]. Five types of DS-CSP system was reviewed by Mancini *et al* [3] at 2003 with system rated power between 9.5~25 kW and SEE value between 19.0%~29.4%. Among them, the Stirling Engine Systems (SES) company 25 kW DS-CSP system got the highest efficiency (29.4%). The SES company established a 150 kW power station in 2005 (rated power is 25 kW), and the SEE of the Serial # 3 can reach to 31.25% on 31 January 2008 and create a new world record [9]. In September 2009, SES company built the first demonstrated plant in Arizona, United States, which was composed of 60-SunCatcher™ dish units with each unit of 25 kW (1.5 MW in total). The plant started production in January 2010 with annual solar-to-electricity gross efficiency equaled to 26% [10]. In year of 2012, a 100 kW DS-CSP demonstration station was built in the Ordos city in Nei Mongolia of China with the unit power of 10 kW. Baharoon *et al* [2] reviewed the development of the CSP technology and presented the DS-CSP power station projects under building or planning (Infinia Corp [12], Capacity 1.5 MW, and start production year 2013). From the recently review[1-3,13,14], most existing DS-CSP systems are with a rated power below 25 kW, but only the SBP company has a system with rated power of 50 kW. Very few literatures have been found for the DS-CSP system rated power between 25 kW to 50 kW which is a power range worth of exploring. In this study, we will develop the rated power 38 kW large DS-CSP system, and future application in the large-scale solar power station or remote areas for distributed power supply.

The development of the DS-CSP system generally includes the design of the Stirling engine, cavity absorber, and the parabolic dish concentrator [13]. The Stirling engine development process includes the mechanical structure design [15,16] (e.g, the design of the piston motion mechanism, regenerator and cooler), thermodynamic calculation [17], fluid dynamics analysis [18], and the design of the generator and control system. This is a complex project. In this paper, a mature Stirling engine (Stirling Biopower Flexgen S260) was applied to the 38 kW DS-CSP system development. The S260 Stirling engine is α-type four cylinders double-acting Stirling engine and working fluid is hydrogen. The S260 Stirling engine was originally applied to biomass thermal power generation, and its heat absorber is enclosed cylindrical cavity structure. We need to redesign the absorber structure in order to apply the S260 Stirling engine to the solar thermal power generation.

In this study, a rated power 38 kW DS-CSP system was developed and tested. The heat engine adopted the alpha-type four cylinders double-acting Stirling engine (Stirling Biopower Flexgen S260). The 17.70 m parabolic dish concentrator has been designed and implementation. The paper structure and main contents are as follows. In section 2, the flux distribution of absorber simulation was conducted by using ray tracing model for analyzing. In section 3, the single dish plus single pillar supporting parabolic dish concentrator system was designed. In section 4, the installation of the concentrator mirror and optical performance test of the concentrator were described. In section 5, the operation data of the 38 kW DS-CSP system were analysed. Lastly, a summary and conclusions were drawn.

2. Absorber flux distribution

The parabolic dish concentrator parameters (radius and focal length) determination needs to consider the performance matching of the concentrator and the Stirling engine. This includes two aspects, one is that the concentrator should provide enough solar energy for the Stirling engine, which means energy matching of the concentrator and the Stirling engine. The other is that the absorber flux distribution needs to be reasonable.

2.1. Basic parameters of dish concentrator

The global coordinate system *O-xyz* is built at the top of point *O* on the parabolic surface, the *z* axis points to the focal point F. The surface of the reflect mirror can be defined as $x^2 + y^2 = 4fz$, where f is

focal radius.

The concentrator structure composed of twelve truss beams in uniform distribution. The mirror is not installed between the two truss beams in the below part to avoid the mechanical interference between the concentrator and the supporting pillar (diameter 800 mm). The angle θ_m is 30 °. The supporting truss was fixed on the concentrator centre position. The mirror can't be installed in this centre position (the corresponding radius R_2=0.90 m). While the section size of Stirling heat engine is 1200 mm×1400 mm (wide × high, Figure 1), the shadow caused by the Stirling engine is located in the circular area radius, which can not cause additional shadows for the reflection mirror. There is a certain gap between the concentrator mirror units. This gap is 20 mm along the radius direction and 25 mm along the circumferential direction which means reflection mirror gap rate k_m is 0.15, and the convenience of mirror installation and also reduces the wind load by allowing part of the wind passing through the gap (figure 4(a)). The effective concentrator aperture area A_{dish} is expressed as:

$$A_{dish} = \frac{2\pi - \theta_m}{2}(R_1^2 - R_2^2)(1 - k_m) \tag{1}$$

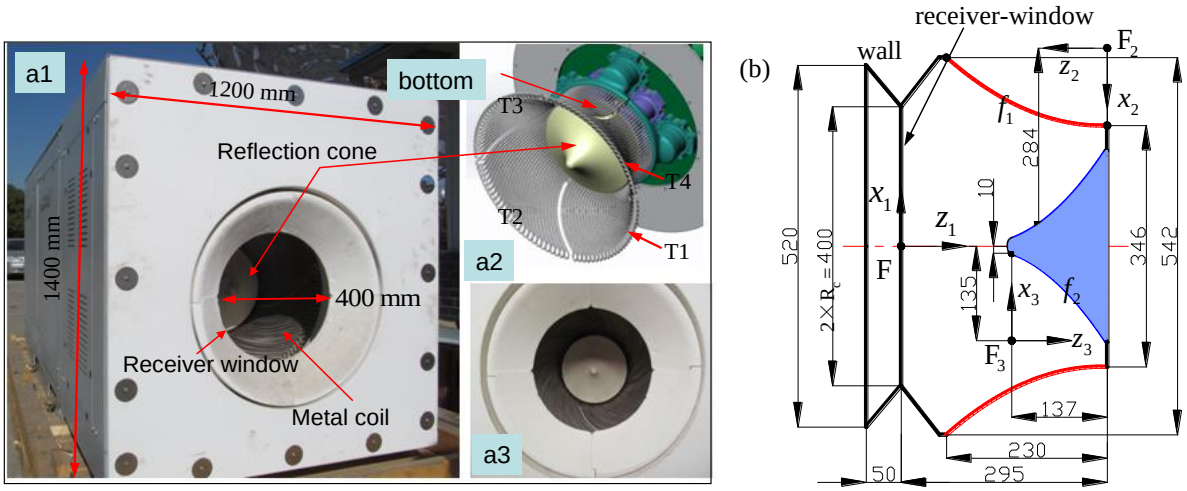

Figure 1. Structure and geometrical parameters of the heat absorber: a1) picture of the Stiring Biopower Flexgen S260, a2) CAD design model of the heat absorber, a3) picture of the heat absorber front view and b) geometrical parameters of the heat absorber.

According to the energy conservation equation (input energy equals output energy) of the DS-CSP, the rated power E_{Ra} is given as:

$$E_{Ra} = A_{dish} \cdot W_0 \cdot \eta_{DS} \tag{2}$$

Where W_0 is the direct normal irradiation (unit is W/m^2); η_{DS} is the designed value of the DS-CSP solar-to-electricity efficiency (SEE).

In this work, the 38 kW DS-CSP system will build in the Xiangtan electric group factory, China (east longitude 112.95 °, north latitude 27.87 °). The Xiangtan region solar irradiation ability has been evaluated and finally determined the DNI design value is 750 W/m^2. The operated DS-CSP system SEE value (19.0%~29.4%) [1-3] has been referenced and the η_{DS} will be directly set at 25% that is a typical efficiency value in the DS-CSP system engineering applications. So the concentrator radius R_1 is selected as 8.850 m to achieve a rated power of 38 kW for the DS-CSP system.

2.2. Structure and parameters of the absorber

In this paper, an engine with four cylinders double-acting Stirling engine and hydrogen as the working

medium (Stirling Biopower Flexgen S260, α-type) is used. The absorber structure parameters are shown in Figure 1 and the absorber are composed of a metal coil and a secondary reflection cone.

The flux distribution of absorber is conducted using a simulation software OptisWorks 2012 based on Monte Carlo Ray Tracing Method [19,20]. Due to the metal coil arranged densely in the absorber and the tube diameter is small, hence it is difficult to directly calculate the flux distribution on the metal coil surface. In this research, the metal coil is simplified into a red surface f_1 and the secondary reflection cone is simplified into a gray surface f_2. In Figure 1(b), the coordinate system F-$x_1y_1z_1$ parallels to the coordinate system O-xyz is established on the focal point F. The coordinate system F_2-x_2z_2 and F_3-x_3z_3 are established respectively for calculating the generating lines of the metal coil and the secondary reflection cone and can be expressed as:

$$x_2 = -0.0020(z_2)^2 + 0.0337z_2 + 111.12 \tag{3}$$

$$x_3 = -0.0042(z_3)^2 - 0.3730z_3 + 125.41 \tag{4}$$

2.3. Absorber flux distribution

The solar half angle 4.65 mrad is considered in this study. We assume the absorption rate of the metal coil surface is 0.75 and reflectance of the cone surface is 0.70 and W_0 is 800 W/m^2. The concentrator reflection mirror using the thickness 4.0 mm silver mirror glass and reflectivity is 0.95. The totally ray tracking number is 20 Mrays during the calculating process according to the independence study. The results of the absorber flux distribution are shown in Figure 2 and Figure **3**.

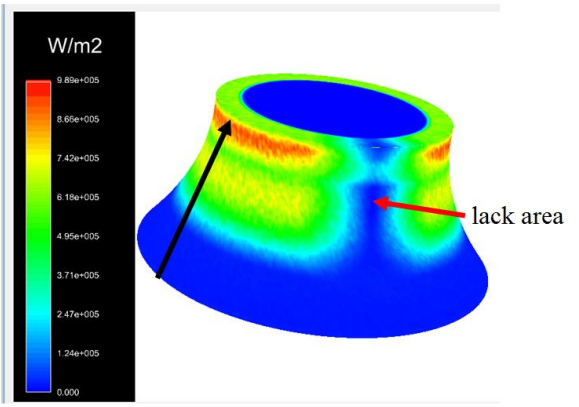

Figure 2. The flux distribution on the metal coil surface in heat absorber (R_1=8.85 m, f=9.49 m).

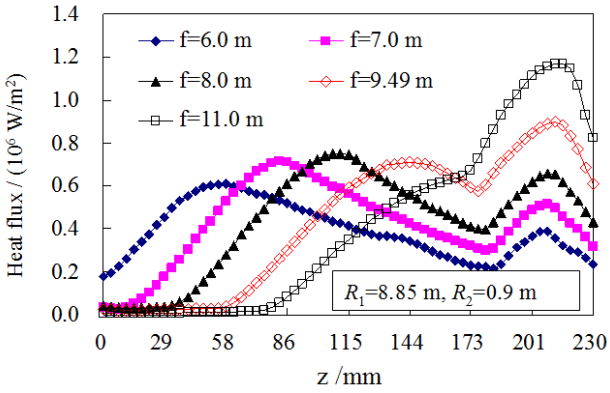

Figure 3. The flux distribution on the metal coil surface (the cross section where the arrow is).

As seen from Figure 2, the 'lack area' exists in the metal coil surface flux distribution, which is resulted from the existence of θ_m. The solar energy is concentrated on the bottom area of the metal coil (Figure 1(a)), which shows two peaks distribution (figure 3). Figure 3 is the flux distribution of the cross section where the arrow is shown in Figure 2. The concentrator radius and focal length significantly affect the flux distribution on the metal coil surface, but still has two peaks distribution characteristics. The focal length is larger and metal coil surface energy is more concentrated to the bottom area when the dish concentrator radius is fixed. This is easy to form the flow stagnation zone at the bottom area, which in turn reduces the convection heat loss. Considering the weight of the Stirling engine (~1600 kg), larger focal length f will lead to significant deformation of the support truss which will further affect the absorber receive the solar energy. Finally, we select the concentrator focal length f is 9.49 m (rim angle is 50 °) when the dish concentrator rim angle is approaching to 45 °.

3. DS-CSP system frame structure design

Dish concentrator frame structure was mainly used to support the reflection mirror and Stirling engine

for realizing the concentrator tracking the sun position. This frame structure design includes the concentrator structure, supporting structure, Stirling engine supporting structure and two-axis tracking mechanism. In this paper, such factors as the manufacturing, construction, maintenance and environmental climate (such as wind and dust) are comprehensive considered by us. The 17.70 m single dish plus single pillar supporting parabolic dish concentrator system was designed.

3.1. Concentrator selection

In the design of the big dish concentrator structure, the SBP Company used single dish concentrator with tensioned membrane structure [9], which ensured a high quality mechanical structure while the concentrating performance under wind load is difficult to guarantee. This makes the structure difficult to be implemented in the windy climate area in China. The use of the multi-surface dish concentrator can increase the drafty performance [20],[22], but the gap among the mirror units reduced the active concentrating areas. In order to guarantee a certain concentrating area, space size of concentrator will be larger which is not suitable for large concentrators.

Therefore, we choose the single parabolic surface concentrator which normally consists of the rectangle or sector mirror unit (use glass reflective mirror). Using rectangle mirror units can generally form an approximate parabolic surface concentrator, such as the Serial #3 unit in SES Company [2]. However, the sector mirror units could ensure a accuracy parabolic surface concentrator [23],[24], which can effective reduce the number and the type of the concentrator mirror units. Such as the SunCatcher^{TM} unit improving designed by the SES company, the number of the mirror units are only 40 [2]. In this paper, our single concentrator will use this sector mirror unit (Figure 4(a)).

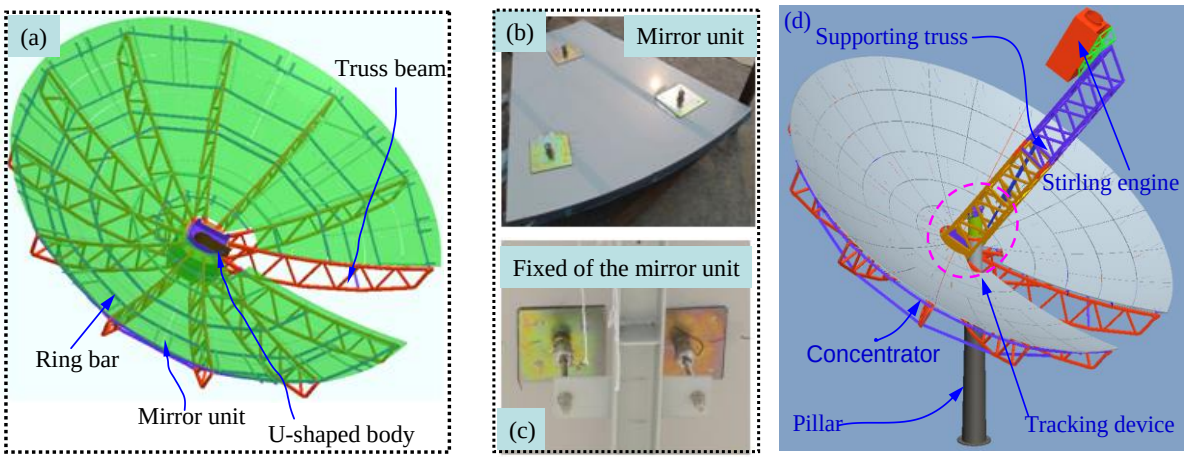

Figure 4. DS-CSP frame structure: a) CAD design model for the concentrator, b) mirror units structure, c) installation of the mirror unit, and d) CAD image of the DS-CSP system.

3.2. Supporting structure selection

Regarding the support structure of the dish concentrator system, the large dish concentrator usually uses the disk rail support due to the superior bearing characteristics in existing literatures [9][25][26]. For example, the Australian National University successively established a 400 m^2 and a 500 m^2 dish concentrator [25][26], and the SBP company implemented the 50 kW DS-CSP unit with such support structure [9]. The disk rail has advantages in stress characteristics. However, the disk rail support still has some disadvantages. For instance, the structure should be protected from the dust and sand and additional weights are needed to balance the dish concentrator system. While the single pillar support form shows advantages in easy construction and good sealing performance, which requires less maintenance and the balance of the system can be easily achieved by the structure parts mass optimize allocation. Due to the advantages of such structure, it is widely used in various CSP projects [2,3]. Hence, the 38 kW DS-CSP system in this study also utilize the single pillar support (Figure 4(d)).

3.3. Structure design of dish concentrator system

Modular design is considered in present study in order to have convenience in manufacturing, transportation, and installation. Concentrator is connected with twelve truss beams to the centre U-shaped body by bolt (Figure 4(a)). The adjacent truss beams are connected through the ring bar which further forms a space truss structure to support the mirror units. Mirror unit is an aluminium honeycomb panel matrix with polyurethane pasted on the upper surface. The polyurethane is bended into parabolic surface with the reflection mirror surface adhesive to the polyurethane surface (Figure 4(b)). This structure can improve the rigidity of the mirror unit structure. The mirror unit is fixed in the space truss structure by the ball joint bolt and the space position of the mirror unit is controlled by adjusting the length of the bolt (Figure 4(c)).

The single dish plus pillar supporting structure is designed for the DS-CSP system and is shown in figure 8(d). The front end of the supporting truss is fixed on the concentrator U-shaped body. The Stirling engine is installed at the end of the supporting truss (absorber is at the focal position of the concentrator), and the supporting truss is connected with the tracking device mounted on the top of the pillar. The tracking device uses the elevation angle plus azimuth angle two-axis tracking method (Figure 4(d)). The tracking device is a combination of the azimuth angle rotating mechanism and lead screw expand and contract mechanism. Both of these two mechanisms are equipped with worm-gear motor to lock the frame structure when the external load applied. The specialty of this design is that the lead screw is jointed at the lower part of the pillar (normally at the top of the pillar, Serial#3 unit for example [2]). The novel design could lead to the benefit that the lead screw will not cover the focal axis of the concentrator and it is convenient for the calibration of the concentrator focal axis when the Stirling engine is installed. Moreover, it can increase the lead screw expand and contract mechanism transmission angle which in turn reduce the push-pull force of the lead screw.

It is crucial to make sure that there is no mechanical interference between the lead screw and the support truss when the lead screw is expanding and contracting. The concentrated system gravity center should be coincidence with the supporting pillar axis which could be achieved by optimizing the allocation of the total mass weight of the concentrator and the supporting truss. This can be effectively obtained in the Pro/E software platform. The main parameters of the DS-CSP frame are shown in table 1.

Table 1. The main parameters and performance index for the 38 kW DS-CSP system.

Name	Numerical or model
System design value	Rated power is 38 kW, DNI design value is 750 W/m^2, solar-to-electricity efficiency design value is 25%.
Stirling system	Stirling Biopower Flexgen S260, α-type, four cylinders double-acting Stirling engine, working medium is hydrogen, mass is 1600 kg, receiver window diameter is 400 mm.
Dish concentrator	Aperture area is 204 m^2, diameter is 17.70 m, focal length is 9.49 m, rim angle is 50.0 °
Number of mirror units	164
Total mass	25.2 tons (Do not include the foundation)
Tracking mode	Elevation-azimuth double-axis tracking device, open loop control system
Output function	Net power output=0.1003×DNI-36.129; DNI∈[460, 761] W/m^2
Peak power	40.5 kW (The effective total aperture area is 200 m^2, DNI is 761 W/m^2, and SEE is 26.9%)

4. Concentrator system installation and test

4.1. Installation of the mirror unit

The optical performance of the concentrator is directly decided by the precision of the mirror unit installation. A laser positioning device is used to guide the installation of mirror units (Figure 5(a)) and the schematic of the laser device are shown in Figure 5(b).

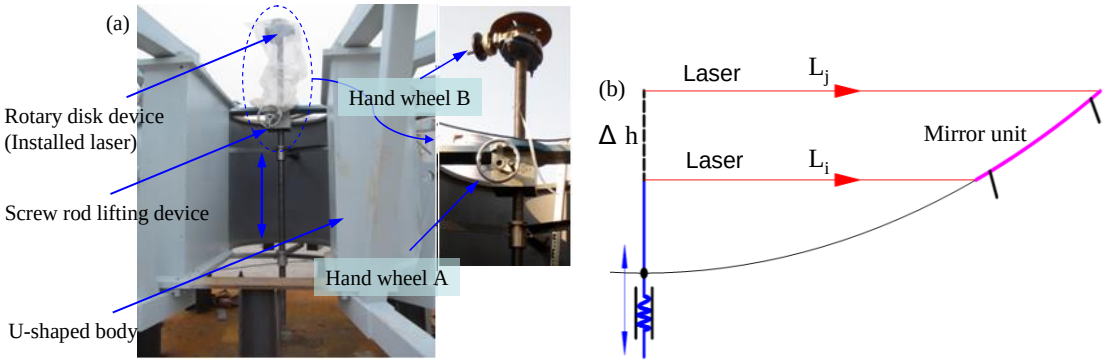

Figure 5. The installation and positioning of mirror units: a) laser positioning device and b) working principle.

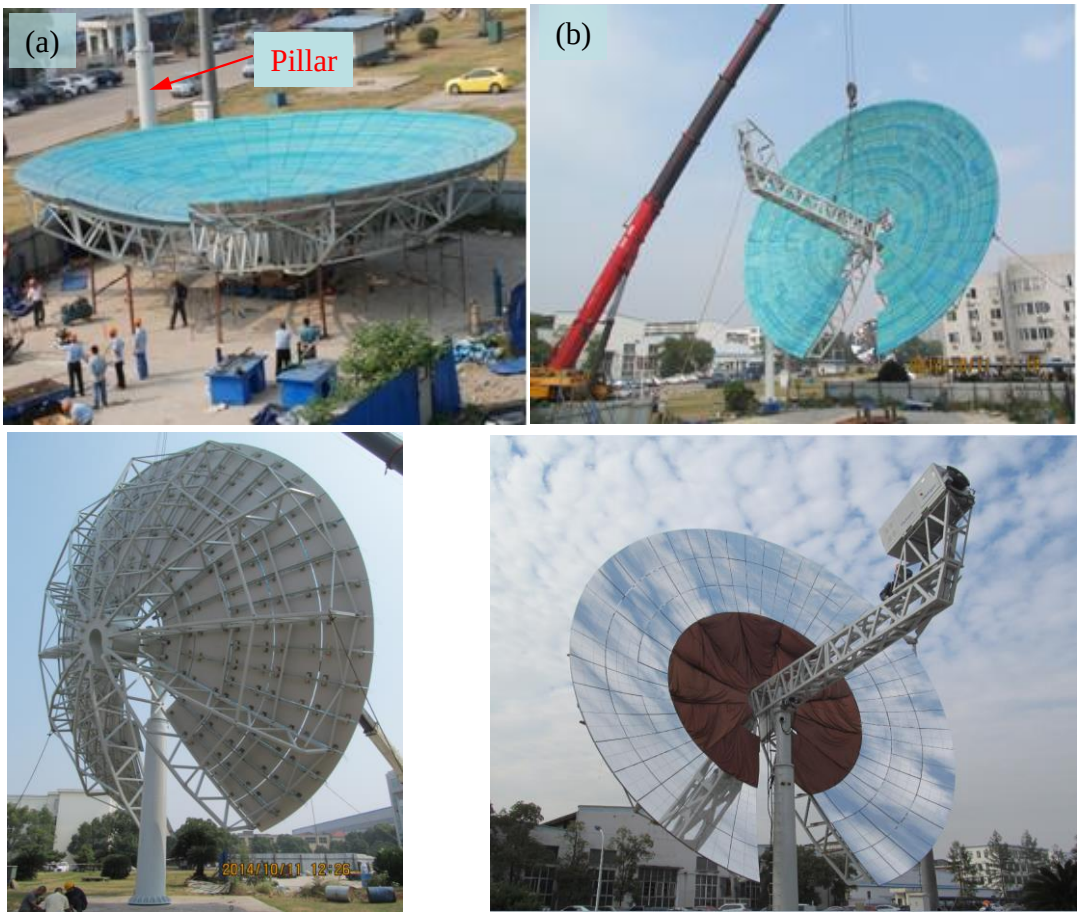

Figure 6. The construction site: a) mirror units installation, b) connecting process of concentrator to the pillar, c) rear view and d) front view.

The detailed implementation steps are as listed follows: 1) pose concentrator truss structure open upward and mark the about-to-install parabolic mirror's focal axis (Z-axis). The make the screw axis

coincidence with the z-axis and fix the laser device on the center of the U-shaped body, 2) rotating the hand wheel A to lift up or down the screw to mark parabolic reflection mirror surface top point (the origin of coordinate O) and then rotate the hand wheel B to point the original position (X-axis) at the parabolic reflection mirror surface (hand wheel A and hand wheel B also have the rules that can accurate fix the desired position), 3) adjust the hand wheel A and B to make laser beam align to the install mirror angular point to the ideal installation mirror unit position, and 4) tune the length of the mirror unit ball joint bolt to make sure that the angular point of the mirror unit is aimed at the laser beam. Repeat the step 3) and step 4) to determine the position of the four mirror unit angular points to complete the installation of the mirror units. Once all the mirror units are installed (Figure 6(a)), fixing the concentrator with the support truss and then combine them with the tracking device on the top of the pillar (Figure 6(b)). The pillar is mounted around the concentrator construction area (Figure 6(a)). The DS-CSP system is built in the factory of the Xiangtan Electric Manufacturing Group (Figure 9).

4.2. Concentrator performance test

4.2.1. Flux distribution on focal plane. In order to determine the concentrator of the focal spot distribution and tracking performance, the simple and effective method is to install a flat receiver in the concentrator focal plane [25] for receiving the solar energy reflected from the concentrator (to form a focal spot). The performance of the concentrator was evaluated by the focal spot brightness distribution and geometrical shape.

In this paper, a water-cooled circular target (diameter is 720.0 mm) is designed to calibrate the focal plane in terms of test the focal spot geometry and two-axis tracking performance (Figure 7). Under the sun tracking condition, a CCD camera (Sony A99) is used to take focal spot image from the water-cooled target plane (Figure 7(c)). Since the water-cooled target surface is lack of Lambert features, we can't precisely know the absolute focal spot flux distribution. However, it is sufficient for us to investigate the geometry and size of the focal spot. The results show that the focal spot is in approximate circular shape and the focal spot center is coincident with the center of the water-cooled disk target. This indicates that the sun tracking performance is well (the tracking control is open loop based on the astronomical algorithm). The diameter of the focal spot flare highlighted area is 272.0 mm (not including the halo area) which is less than the diameter of the absorber receiver window (R_c=400 mm). The absorber can receive most of the concentrated solar energy which can be proved in Figure 9.

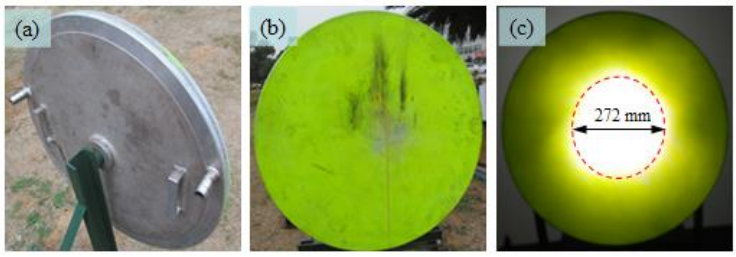

Figure 7. Pictures of the water-cooled target test: a) water-cooled target back view, b) water-cooled target front view, and c) focal spot (focal plane position).

4.2.2. Flux distribution on absorber imitation device. The absorber metal coil flux distribution homogeneity performance influenced the Stirling engine running performance, which including two aspects: (1) the absorber metal coil is composed of four integrated tubes (Figure 1 a2), each integrated tube connected with one Stirling engine piston chamber for providing energy to the piston movement. When four integration tubes receive the difference total heat, the four piston thrust will be different which can cause unstable phenomenon in the S260 Stirling engine operation process. Therefore, the requiring of the four integration tubes receiving the equal total energy. This is a macro requirement for

the metal coil flux distribution homogeneity. (2) The metal coil working in high temperature and high pressure environment. But the metal coil hydrogen working medium heat exchanging ability is limited, the local metal coil area receiving too much energy will cause the metal coil burning or the thermal stress fracture accident caused by large temperature gradient [24]. Hence, the microcosmic requirement for the flux distribution homogeneity on the metal coil is to avoid local "hot spots".

However, water-cooled target experiment can determine the focal plane flux distribution and it can not reveal the absorber flux distribution on the metal coil surface. Therefore, in order to ensure the safe and smooth operation of the S260 Stirling engine, we put forward a new method for evaluating the absorber surface energy distribution. An absorber imitation device (metal material is Q235) is designed and implemented based on the shape of the S260 Stirling engine absorber cavity (Figure 1(b)). The absorber imitation device is installed on the focal position of the dish concentrator (figure 12(a)) and heating performance test (Figure 8(b) and Figure **8**(c)) was conducted. It can be seen that melting was detected on the surface of the absorber imitation device and local surface temperature could be larger than 1493 ℃ (the metal Q235 melting point is 1493 ℃). The brightness distribution within the absorber imitation device has the similar behaviour with the results shown in Figure 2(a) and the energy mainly focus on the absorber bottom area. The absorber inner surface receiving the solar energy distribution is a circular, the energy distribution is homogeneous and without obvious local “bright spot”, which reached to the absorber energy uniformity requirements. Besides, the brightness distribution in Figure 8(c) shows that the reflection cone area has the extremely lower irradiance due to the reflective cone surface reflected the incoming sunlight into metal coil surface and increase the energy of the metal coil surface which shows the functionality of the reflection cone.

It indicates that both the installation precision and two-axis tracking precision of the dish concentrator system meet the operating requirements and Stirling engine can be installed and then the DS-CSP system can make trial operations.

Figure 8. Test of the absorber imitation device.

5. Power generation operation and analysis

The Stirling engine can be started only when the absorber working temperature is high enough (400℃ for the hydrogen (working fluid of the engine) for the 38 kW DS-CSP system in present study) which is the precondition for the operation of the DS-CSP system.

As shown in Figure 9, the first field test of the 38 kW DS-CSP system was conducted on 19th December 2014 with the two inner loops of the mirror covered with shelters. Due to the discontinuity of solar irradiation resulted from the clouds on that day, the hydrogen temperature will decrease accordingly and the Stirling engine will stop when the hydrogen temperature is lower than 400℃. The Stirling engine will be started again then the hydrogen temperature in the metal coil is up to 400℃ once the cloud passing away. A series of the Stirling engine start-stop process prove that the 38 kW DS-CSP system can automatic fit cloud cover weather. The Stirling engine automatic start-stop process in controlled by control system and the automatic control is depended on the feedback of the metal coil hydrogen temperature. The absorber detailed picture during the working condition is given in Figure 9 which can be seen that most of the absorber aperture could capture most of the concentrated solar irradiation. The adjustment and stable test of the DS-CSP control system are accomplished in 8 months. The relationship between the DS-CSP generation power and the DNI is

measured and presented in figure 10 under clear weather with the total concentrated area is 200 m^2 (real time the DNI measurement is achieved by using the GEONICA METEODATA-3000 system, this system was from Geonica company). The main parameters and performance index for the 38 kW DS-CSP system is shown in table 1.

Figure 9. Pictures for the DS-CSP system power operation for the first time (19 December 2014).

As seen from the power generation curve of the DS-CSP system in figure 10(a) (October 26th, 2015), the DS-CSP system continuous operation for 6.5 hours and the power generation is larger than 35 kW during the time from 11:00 to 15:00 (excluded the cloud cover time). When the DNI maximal value is 761 W/ m^2 the DS-CSP system power can reach up to 40.5 kW and the SEE is 26.6% (at 13:25). In the figure 10(b) (October 15th, 2015), during the time period of 11:00 to 13:10, the DNI basically stabilized around 750 W/m^2 and the DS-CSP power value is larger than 38 kW and SEE is 25.3%. The DS-CSP system testing operating SEE value is higher than the design value 25%. Results show that the concentrator design can effectively match the S260 Stirling engine power and the design of the absorber for such Stirling engine is reasonable, which also validates that the S260 Stirling can be well coupled to a solar dish concentrator for power generation. In addition, the concentrator has some optical losses due to the dust coverage, which indicates that the DS-CSP system could achieve even higher SEE. Note that when the elevation angle is small the DS-CSP system will be shadowed by the nearby buildings that the DS-CSP system can only operate up to 15:41 in figure 10(a).

According to the operating data, the relationship between the DS-CSP system net power output and the DNI value is obtained in figure 10(c). The data originated from four days' operation (8th, 15th, 17th, and 26th October 2015) and the unstable data are not included during the Stirling engine shut-up and shut-down. It can be seen that the DS-CSP system net power output has linearly proportional relationship with the DNI value, and this is the same to the DS-CSP system power output curve fitted by Mancini *et al* [3] (DS-CSP system power output curve comparison can be seen in Figure 11). The 38 kW DS-CSP system net power output fitting linear function is y=0.1003x-36.129, where y is the net power output of the DS-CSP system (unit is kW), x is the DNI value. The range of the x is between 460 W/m^2 to 761 W/m^2 (figure 10(c)). This net power output function can be used for 38 kW DS-CSP system output power under different DNI values. Only when we know the power station region solar irradiation data throughout the year can we evaluate the annual power generation according to the net power output function and then assess the economy of the power station construction and operation. This is a very important evaluation work during the early construction period of the business DS-CSP system.

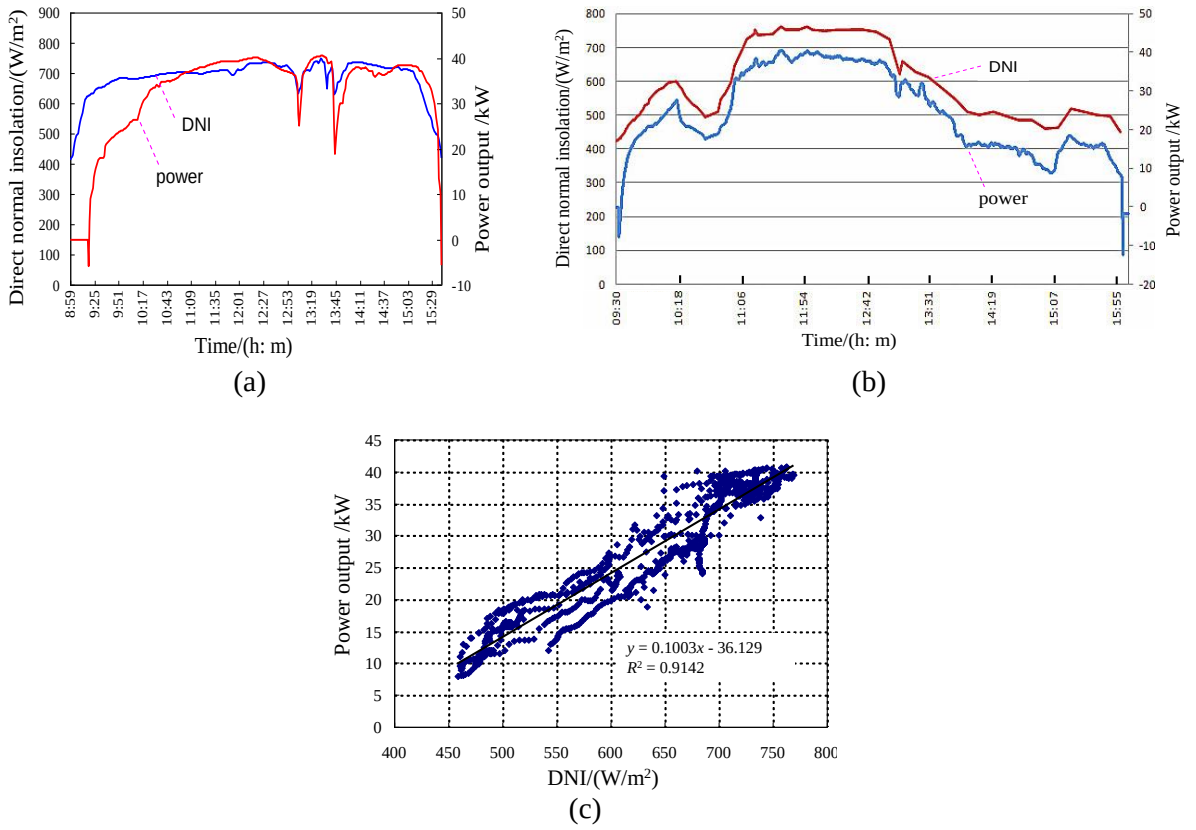

Figure 10. Operating data for the 38 kW DS-CSP system (concentrated area is 200 m2): a) power generation curve on October 26th, 2015, b) power generation curve on October 15th, 2015, and c) DS-CSP power generation curves for 8th, 15th, 17th, and 26th October 2015.

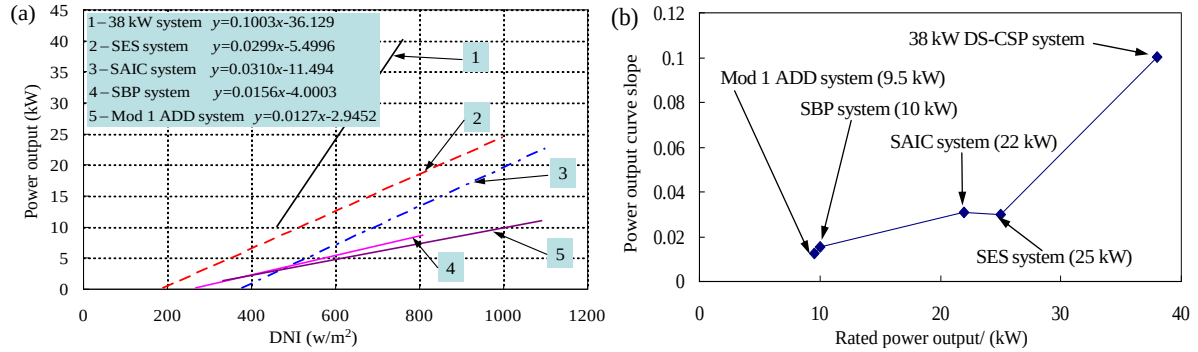

Figure 11. DS-CSP system power output curve comparison: a) power output curves for various systems, and b) power output curve slope comparison. The curves are all acquired form literature (Mancini *et al* [3]) and the test data for our 38 kW DS-CSP system was obtained from the date (8th, 15th, 17th, and 26th October 2015). Where x is the DNI value and y is the power output of the DS-CSP system, the range of x is between the line's both endpoints respectively.

In Figure 11(a), the 38 kW DS-CSP system net output power reached to 38 kW when the DNI value was 750 W/m^2 and the absorber metal coil would be overheated-damaged when the DNI value was over 750 W/m^2, while other four kinds of DS-CSP system could reach the rated output power only when the DNI was about 1000 W/m^2. The Stirling engine has not been full played when the DNI value was less than 1000W/m^2. Since the DNI value is changing with the time, the absorber metal coil

overheated and the Stirling engine lack of heat supply problems would happen. For the metal coil overheated problem, we have figured out a solution: installing the glass cover on the cavity absorber (Figure 1 a1) receiver window position to form a closed space in the absorber. When the metal coil temperature is high, pump the air into the absorber to properly cool the metal coil (made the cold air into one side of the absorber cavity, made the hot air out of the other side). The outflow hot air could also be used to heat the water that can achieve the solar power joint supply. This case could fit the single family or farm offering electric power and heating. Besides, developed the absorber with energy storage function is the best way to solve this problem, because it will not only satisfy the commercial power station energy storage requirements of DS-CSP systems but also could solve the absorber energy overheated-damaged problems. For the DS-CSP system lack of solar energy supply problems, it could be solved by the method of gas and solar energy complementary power generation. The key is to design an absorber that not only could receive the solar energy but also could receive the heat from the gas combustion.

6. Conclusions

In this paper, the rated power 38 kW DS-CSP system was developed. The parabolic concentrator aperture area is 204 m^2 with 8.85 m in radius and 9.49 m in focal length and the heat engine adopted the Stirling Biopower Flexgen S260. This paper forms a general method and process of the structure design, mirror installation and optics testing, which could provide the reference for the DS-CSP system design and development. The outcome has been concluded in the following points:

The 38 kW DS-CSP system has a well recorded working performance which shows the net output power as high as 38.0 kW under the DNI of 750 W/m^2 and the SEE of 25.3% accordingly. The maximum recorded net output power is 40.5 kW and the corresponding SEE is 26.6% with measured DNI of 761 W/m^2.

The net power output of the 38 kW DS-CSP system is linearly proportional to the DNI value and the fitting function is Net power output=0.1003×DNI－36.129, DNI∈[460, 761] W/m^2. The linear function can predict the annual total generation power of the 38 kW DS-CSP system, which could guide the DS-CSP system station construction economic evaluation.

The absorber imitation device testing method was presented, which could assess the flux distribution on the absorber cavity surface. The test results show that the brightness distribution within the absorber imitation device has the similar behaviour with the absorber flux distribution simulation result and the energy mainly focused on the absorber bottom area. While the reflection cone area reports much lower luminance, the reflection cone could effectively reflect the incoming sunlight into metal coil surface and this could conducively improve the absorber thermal efficiency.

7. Future work

The space size and mass of the dish concentrator in DS-CSP system are large. The structure deformation is easy to occur under the effect of wind load and gravity load further to affect the optical performance of the dish concentrator [27]. In order to reduce the mass and manufacturing cost of dish concentrators, it is necessary to carry out lightweight design of the frame structure on the basis of ensuring optical performance. Next, in the large-scale DS-CSP power station, the proximity of the DS-CSP system will generate light shading and cloud cover against the sunlight, which will affect the normal operation of the DS-CSP system. Therefore, the layout optimization of the DS-CSP system in large-scale power stations is especially important. Besides, large dish concentrators are usually assembled with many mirror units forming the parabolic reflecting mirrors and each mirror unit must be accurately fixed in a present position within the truss structure. If facet alignment error exists after the mirror unit is installed, the shape accuracy of the parabolic concentrator surface can be affected [28]. Therefore, correctly aligning the mirror units in dish a concentrator while minimizing installation error is therefore of great importance to overall performance. The development of an effective mirror alignment method or alignment tool to guide mirror facet alignment during operation would be extremely valuable [29].

Acknowledgments
This work is supported by the National Natural Science Foundation of People's Republic of China (No. 51576061, 51641504), Hunan Province Natural Science Foundation of People's Republic of China (No. 2016JJ2052), and Hunan Province Postgraduate Innovation Project Foundation of People's Republic of China (No. CX2016B549, CX2017B628).

References

[1] Poullikkas A *et al* 2010 Parametric analysis for the installation of solar dish technologies in Mediterranean regions *Renew Sust Energ Rev* **14** 2772-83
[2] Baharoon D A *et al* 2015 Historical development of concentrating solar power technologies to generate clean electricity efficiently–A review *Renew Sust Energ Rev* **41** 996-1027
[3] Mancini T *et al* 2003 Dish-Stirling systems: An overview of development and status *J Sol Energy Engineering* **125** 135-51
[4] Bravo Y *et al* 2012 Environmental evaluation of dish-Stirling technology for power generation *Sol Energ* **86** 2811-25
[5] Sandia 2004 Stirling to build solar dish engine power plant, goal is to deploy solar dish farms with 20,000 units producing energy https://share.sandia.gov/news/resources/releases/2004/renew-energy-batt/Stirling.html
[6] Karabulut H *et al* 2009 An experimental study on the development of a β-type Stirling engine for low and moderate temperature heat sources *App Energ* **86** 68-73
[7] Stine W B 1993 International survey of parabolic dish/Stirling engine electrical power generation technology *ASME* (New York, USA) 421-7
[8] Stine W B and Diver R B 1994 A compendium of solar dish/Stirling technology (No. SAND93-7026) *Sandia national labs albuquerque NM*.
[9] Koshaim B 1986 Report: Fifty KW solar Membrane Concentrator *The SOLERAS Program, Saudi Arabian National Center for Science and Technology*
[10] News Releases 2008 Sandia, Stirling energy systems set new world record for solar-to-grid conversion efficiency https://share.sandia.gov/news/resources/releases/2008/solargrid.html
[11] Maricopa Solar Project 2013 http://www.nrel.gov/csp/solarpaces/project_detail.cfm/projectID=58
[12] Directory: InfiniaCorp 2016 http://peswiki.com/directory:infiniacorp
[13] Hafez A Z *et al* 2016 Solar parabolic dish Stirling engine system design, simulation, and thermal analysis *Energ Convers Manage***126** 60-75.
[14] Hafez A Z *et al* 2017 Design analysis factors and specifications of solar dish technologies for different systems and applications *Renew Sust Energ Rev* **67** 1019-36
[15] Cheng C H and Yang H S 2012 Optimization of geometrical parameters for Stirling engines based on theoretical analysis *App Energ* **92** 395-405
[16] Hooshang M *et al* 2015 Optimization of Stirling engine design parameters using neural networks *Renew Energ* **74** 855-66
[17] Ahmadi M H *et al* 2017 Thermal models for analysis of performance of Stirling engine: A review *Renew Sust Energ Rev* **68** 168-84
[18] Xiao G *et al* 2017 Design optimization with computational fluid dynamic analysis of β-type Stirling engine *App Therm Eng* **113** 87-102
[19] He Y L *et al* 2011 A MCRT and FVM coupled simulation method for energy conversion process in parabolic trough solar collector *Renew Energ* **36** 976-85
[20] Tan M H and Chong K K 2016 Influence of self-weight on electrical power conversion of dense-array concentrator photovoltaic system *Renew Energ* **87** 445-57
[21] Huang X *et al* 2014 Development of a multi-layer and multi-dish model for the multi-dish solar energy concentrator system *Sol Energy* **107** 617-27
[22] Giannuzzi A *et al* 2015 Enhancing the efficiency of solar concentrators by controlled optical aberrations: Method and photovoltaic application *App Energ* **145** 211-22

[23] Wang K *et al* 2015 Experimental study on a coiled tube solar receiver under variable solar radiation condition *Sol Energy* **122** 1080-90
[24] Xiao G *et al* 2016 A model-based approach for optical performance assessment and optimization of a solar dish *Renew Energ* **100** 103-13
[25] Lovegrove K *et al* 2011 A new 500 m 2 paraboloidal dish solar concentrator *Sol Energy* **85** 620-6
[26] Lovegrove K *et al* 2003 Paraboloidal dish solar concentrators for multi-megawatt power generation *ISES Solar World Conference* (Goteborg, Sweden)
[27] Yan J *et al* 2015 Research on thermal-structural-optical multi-field coupling modeling and concentrating performance predication of solar dish system *Journal of Mechanical Engineering (in Chinese)* **51** 138-51
[28] Yan J *et al* 2016 Correlative characteristics between focal spot of solar dish concentrator mirror unit and posture error *Acta Optica Sinica (in Chinese)* **36** 1122003
[29] Yan J *et al* 2017 Solar concentrator mirror unit supporting/adjusting structure and posture alignment *Acta Optica Sinica (in Chinese)* **37** 0522001